Elucidating the assembled structure of amphiphiles in solution *via* cryogenic transmission electron microscopy

Honggang Cui,[a] Travis K. Hodgdon,[b] Eric W. Kaler,[b] Ludmila Abezgauz,[c] Dganit Danino,[c] Maya Lubovsky,[d] Yeshayahu Talmon[d] and Darrin J. Pochan*[a]

Received 20th March 2007, Accepted 31st May 2007
First published as an Advance Article on the web 28th June 2007
DOI: 10.1039/b704194b

For the past twenty years, significant progress has been made in both developing cryogenic transmission electron microscopy (cryo-TEM) technology and understanding assembled behavior of amphiphilic molecules. Cryo-TEM can provide high-resolution images of complex fluids in a near *in situ* state. Samples embedded in a thin layer of vitrified solvent do not exhibit artifacts that would normally occur when using chemical fixation or staining-and-drying techniques. Cryo-TEM has been useful in imaging biological molecules in aqueous solutions. Cryo-TEM has become a powerful tool in the study of *in situ*-assembled structures of amphiphiles in solution as a complementary tool to small-angle X-ray and neutron scattering, light scattering, rheology measurements, and nuclear magnetic resonance. The application of cryo-TEM in the study of assembled behavior of amphiphilic block copolymers, hydrogels, and other complex soft systems continues to emerge. In this context, the usage of cryo-TEM in the field of amphiphilic complex fluids and self-assembled nano-materials is briefly reviewed, and its unique role in exploring the nature of assembled structure in liquid suspension is highlighted.

Introduction

Cryogenic transmission electron microscopy (cryo-TEM) extends the capabilities of TEM by allowing for *in situ* imaging of delicate structures of soft matter, including liquid systems, providing unique information not obtainable by other methods.[1–9] A wide range of length scales can be directly imaged, ranging from a few nanometres to several micrometres. When dissolved in solvents, amphiphiles, including surfactants, lipids, and amphiphilic block copolymers, self-assemble into well-defined structures with an extensive variety of shapes, such as spherical and worm-like micelles, vesicles, lamellar sheets, sponge-phases, nanotubes, networks, disks, toroids, as well as many intermediate and mutative phases. Exploring their assembled nature is of great theoretical and practical value due to their applications in materials science,[10] bioengineering,[11] and the pharmaceutical industry.[12] However, most self-assembled structures are stable only in their native solution conditions including concentration, temperature, pH and the presence of other molecules such as salts. Direct imaging of liquids, including assembled structures in solution, is not possible in a high-vacuum TEM chamber because of the vapor pressure of solvents and molecular diffusion. Complete removal of solvent from the sample often results in the

[a]*Department of Materials Science and Engineering and Delaware Biotechnology Institute, University of Delaware, Newark, DE 19716. E-mail: pochan@udel.edu; Fax: +1 302 831 4545; Tel: +1 302 831 3569*
[b]*Center for Molecular Engineering and Thermodynamics, Department of Chemical Engineering, University of Delaware, Newark, DE 19716*
[c]*Department of Biotechnology and Food Engineering, Technion-Israel Institute of Technology, Haifa 32000, Israel*
[d]*Department of Chemical Engineering, Technion-Israel Institute of Technology, Haifa 32000, Israel*

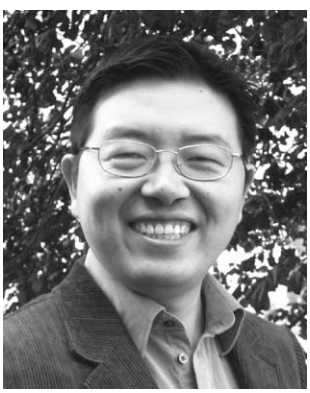

Honggang Cui

Honggang Cui received his B.E. in Polymer Materials Science and Engineering from the Beijing University of Chemical Technology in 1999 and M.E. in Materialogy from the Tsinghua University in 2002. He obtained his Ph.D. in Materials Science and Engineering at the University of Delaware under the supervision of Darrin J. Pochan in 2007. His research interests include block copolymer assembly, polypeptide crystallization and materials characterization.

Travis K. Hodgdon

Travis K. Hodgdon is a Ph.D. candidate in the Department of Chemical Engineering at the University of Delaware under the advisement of Professor Eric Kaler. He obtained his B.S. in Chemical Engineering at the University of Pittsburgh in 2003. His current research interests include the study of microstructure formed in aqueous mixed surfactant and hydrotrope solutions.

deformation or complete destruction of the assembled structure.[12,13] Consequently, in order to successfully examine the native *in situ* structure of self-assembled structures in solution by TEM, one needs to stabilize the volatile solvent and avoid evaporation while preserving the structure.

One method for stabilizing dried aggregates is chemical fixation, which involves the addition of chemicals to react with the assemblies. This method can be problematic because micro- and nanostructured fluids are almost always sensitive to changes in solvent and chemical content. A more favorable

Eric W. Kaler

Eric W. Kaler is a Professor in the Department of Chemical Engineering at the University of Delaware, and is interested in a variety of self-assembly processes involving surfactants, polymers, polyelectrolytes, and soluble and membrane proteins. His laboratory characterizes the materials and the kinetics of their formation with a variety of tools, including scattering and cryo-TEM

Ludmila Abezgauz

Ludmila Abezgauz is a Ph.D. student in Dr Danino's laboratory at the Technion-Israel Institute of Technology. Her present research examines the growth laws that control the nanostructure of assembled surfactants and polymers in solution, and combines direct-imaging and freeze-fracture cryo-TEM with a range of spectroscopic and calorimetric techniques.

Dganit Danino

Dganit Danino received her Ph.D. in Chemical Engineering from the Technion-Israel Institute of Technology. After 4 years as a research associate, she performed post-doctoral research at the Laboratory of Cell Biochemistry and Biology at NIDDK, NIH for 2 years. In 2002, Dr Danino joined the Biotechnology and Food Engineering Department at the Technion. She is interested in mechanisms of self assembly in colloidal and biological systems. Her work is highly focused on the development and application of cryo-TEM techniques in studying the dynamics and nanostructure of molecular assemblies and complex fluids.

Maya Lubovsky

Maya Lubovsky earned a B.Sc. in 2006, and is working on her M.Sc. in Chemical Engineering at the Technion-Israel Institute of Technology. She studies reverse thread-like micelles in non-aqueous systems by direct-imaging cryo-TEM (DICT) and freeze-fracture-replication transmission electron microscopy (FFR-TEM).

Yeshayahu Talmon

Yeshayahu (Ishi) Talmon is the Wolfson Professor of Chemical Engineering, Technion-Israel Institute of Technology. He is Head of the Technion Project on Complex Fluids, Microstructure and Macromolecules, a Member of the Technion Russell Berrie Nanotechnology Institute, and serves on it's International Scientific Advisory Committee. He has developed and applied cryo-TEM since the late 1970's.

Darrin J. Pochan

Darrin Pochan is currently an Associate Professor in the Materials Science and Engineering Department as well as the Delaware Biotechnology Institute at the University of Delaware. He obtained his B.S. in Chemistry from the University of Wisconsin-Madison, and M.S. and Ph.D. in Polymer Science and Engineering at the University of Massachusetts-Amherst. The Pochan group research program involves the construction of new materials and nanostructures via molecular self-assembly mechanisms. Materials of interest include multicompartment, novel micelles, hierarchically structured hydrogels from peptide self-assembly, and the directed assembly of inorganic nanoparticles.

alternative is the physical fixation of assemblies in solution, which can be achieved by rapidly plunging the liquid dispersion into a suitable cryogen to convert the solvent into a solid-like, glassy state. This method of physical fixation is used in freeze-fracture-replication transmission electron microscopy (FFR-TEM) and in direct-imaging cryo-TEM sample preparation. In FFR-TEM, the rapidly frozen specimen is fractured, shadowed with a thin metal layer by vapor deposition, and coated by a thin carbon film to form a stable metal–carbon replica. Metal shadowing gives strong contrast, while the carbon backing provides mechanical stability to the replica. The sample itself is then cleaned away and the metal replica imaged by TEM at room temperature. In contrast, cryo-TEM relates to *direct* imaging of the vitrified liquid specimen.

Cryo-TEM can potentially be applied to most liquid solvents; however, the majority of samples studied are aqueous. Only a limited, although increasing, number of cases involving organic solvents have been reported to date.[14–30] Preparation of a cryo-TEM sample includes three major steps (Fig. 1): (1) applying the liquid onto a perforated carbon film supported on a TEM copper grid, or, sometimes, on a bare metal grid; (2) blotting the grid with solvent-absorbent filter paper; and (3) rapidly plunging the grid into a cryogen reservoir. Samples can be applied to a grid by either pipetting a small drop (typically $\sim$5 μl) or by submerging the grid directly in the solution. Blotting is necessary to form a film that is thin enough to allow adequate electron penetration, but thick enough to accommodate the self-assembled structures. Successful grid preparation is more probable if the liquid application, blotting, and plunging take place within a controlled environment vitrification system (CEVS), in which the atmosphere surrounding the grid can be kept at a desired temperature–humidity–solvent saturation level so as to minimize evaporation of the thin sample film before and during plunging. A CEVS system can be built in-house[1] or can be purchased commercially (*e.g.* the Vitrobot from FEI).[31] Usually, vitrified films are less than $\sim$300 nm in thickness.

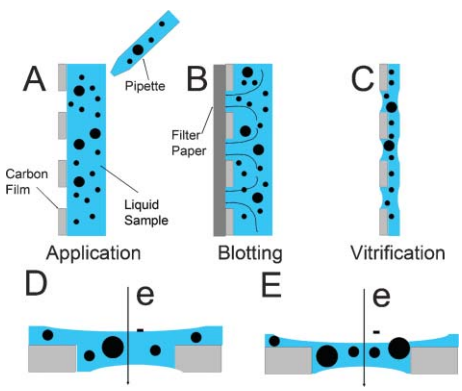

Fig. 1 Schematic of cryo-TEM sample preparation: (A) Side view of a liquid containing particles (●) being applied to a perforated carbon TEM grid; (B) removal of excess solution by blotting grid with filter paper; (C) formation of vitrified thin film after rapidly plunging into a suitable cryogen; (D) expanded side view of vitrified grid showing the path of the electron beam when viewed in a TEM column; (E) size segregation may occur during sample preparation, with larger particles at the edges of the holes and smaller particles at the center of the thin film. Large particles may also protrude from the film.

Once vitrified, the grid is transferred into a liquid nitrogen-cooled cryo-holder. During imaging of aqueous suspensions, the temperature should be kept below −160 °C to prevent the formation of either cubic- or hexagonal ice,[32] and to limit solvent sublimation. Preservation of *in situ*-assembled nano- or micro-structures can be inferred from the quality of solvent vitrification. Molecules like surfactants and block copolymers are not likely to rearrange to form new structures if the (typically smaller) solvent molecules are vitrified during cooling.[2] Liquid ethane is the most popular cryogen used for cryo-TEM, providing a cooling rate of about 10^5 K s^{-1}, as directly measured by Siegel *et al.*[33] Liquid nitrogen, in general, is a poor cryogen due to its narrow temperature range between freezing point and boiling point. Liquid propane is less practical because it is difficult to remove from the vitrified grid due to its low vapor pressure. Table 1 lists the critical properties for the three common cryogens. Another important consideration for choosing a cryogen is the sample solvent solubility in the liquid cryogen. High solvent solubility can be a concern when working with amphiphiles in organic solvents.[14,34]

Contrast in a cryo-TEM image arises from both mass-thickness contrast and phase-contrast mechanisms. Mass-thickness contrast is often insufficient to image amphiphilic systems because many solutes and solvents are comprised mainly of low-atomic-number elements. However, the dense packing of hydrophobic moieties and the presence of any somewhat heavier atoms such as sulfur or phosphorous do contribute to mass-thickness contrast. On the other hand, phase contrast is always an important contrast mechanism for cryo-TEM images. Phase contrast originates from electron-wave interference of unscattered electrons and elastically scattered electrons. Phase contrast can be enhanced by under-focusing the objective lens, which induces a phase shift of the scattered electrons. Assembled nano-objects with inner electron potentials different from the vitreous solvent then become visible. Although maximum phase contrast can be gained with a large underfocus distance, one must be aware that underfocus may be accompanied by loss of resolution and

Table 1 Characteristics of various coolants

Coolant[a]	Temperature at which the coolant has vapor pressure listed below/°C[35] 1 mmHg	760 mmHg (boiling point)	Melting point/°C
Nitrogen (N_2)	−226.1 (solid)	−195.8	−210.0
Ethane (C_2H_6)	−159.5	−88.6	−183.2
Propane (C_3H_8)	−128.9	−42.1	−187.1

[a] Liquid nitrogen is not a good cryogen due to the narrow range between its melting point and boiling point. This produces a thin gas film during quenching that significantly slows the vitrification process. The cryo-TEM operation temperature is typically around −170 °C. At such a temperature, the ethane crust formed during sample preparation readily sublimes or evaporates after the specimen was loaded into high-vacuum TEM chamber (typically 10^{-4} ∼ 10^{-7} Pa or 10^{-6} ∼ 10^{-9} mmHg). Propane has a relatively low vapor pressure, and its crusts are generally visualized as artifacts in cryo-TEM.

the appearance of optical artifacts such as reversed contrast and Fresnel fringes. Consequently, images obtained may not present the true physical size, and it is possible some details are obscured.

Surfactants and lipids

Determination of micellar structure with scattering methods typically involves fitting the scattering spectrum with a model that assumes a micellar shape, or using an indirect Fourier transform method[36] that can give a model-free estimate of micellar shape and size. These methods can lead to ambiguities, especially when samples exhibit unexpected shapes, high polydispersity, or strong inter-particle interactions. In addition, if several distinctively different aggregate shapes exist in solution, the analysis of scattering spectra is even more frustrating. On the other hand, cryo-TEM easily differentiates between topologies that are difficult to resolve by scattering, such as between small disk objects and spherical micelles, or between narrow ribbon elements and cylindrical micelles (Fig. 2).[37] Direct imaging of aggregates in solution can also be critical for reconciling experimental scattering results with theoretical models. Cryo-TEM has been successfully employed to visualize structures ranging from spherical micelles, to worm-like micelles, branches, networks, nanotubes, vesicles, disks and ripple-phase structures, all of which form by the self-assembly of surfactants in aqueous solutions.[2,37–55]

Cryo-TEM has been a valuable tool for the study of vesicles in solution, as it provides a method for determining bilayer thickness and vesicle-size distribution.[38,39] The size distribution of vesicles is important, because it is inherently related to the spontaneous curvature, membrane-bending constant, elastic modulus, and molecular packing parameters of the bilayers, and because it provides insight into the mechanism of vesicle stabilization. It has been proposed that equilibrium vesicle stabilization is the result of either dominating thermal fluctuations or a strong spontaneous curvature.[38,40] Vesicles stabilized by thermal fluctuations are characterized by a significant variation in curvature, resulting in a polydispersed unilamellar population. Vesicles stabilized by a high degree of spontaneous curvature are relatively monodispersed and generally coexist with multilamellar vesicles. Multilamellar vesicles are defined by the additional membrane(s) that exist inside the outmost vesicle membrane.[40] Therefore, the stability mechanism of vesicles can be distinguished by observing the size distribution and presence of multilamellar vesicles.[40]

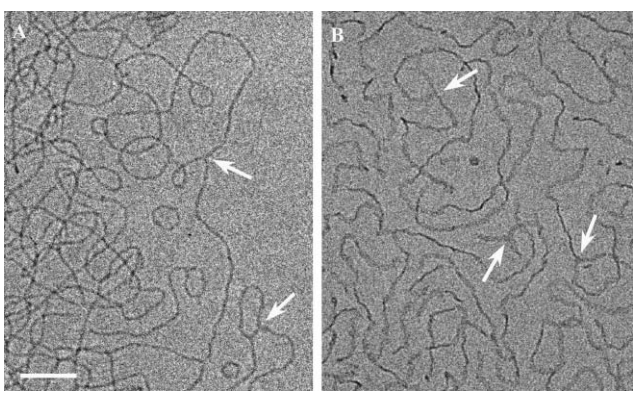

Fig. 2 (A) Thread-like micelles formed in a 1 : 1 molar ratio mixture of octyltrimethylammonium bromide and sodium oleate (total of 3 wt%) at 25 °C. (B) Ribbon assemblies formed in a mixture of 0.4 wt% ethylene glycol monododecyl ether and 1 wt% polyoxyethylene cholesteryl ether at 50 °C. Light and dark segments correspond to ribbon segments perpendicular and parallel to the electron beam, respectively. The white arrows in both panels point to branching points.[37]

It has been postulated that the size polydispersity of vesicles formed in mixed surfactant systems is the result of shear forces that occur during the initial combination of the surfactants.[41] Jung *et al.* claimed this speculation was not the case in the systems they studied, where SANS and freeze-fracture TEM results suggest that the vesicle-size distribution is a thermodynamic property.[39,40] Additionally, Jung *et al.* reported that oddly shaped bilayer structures can coexist with almost uniformly spherical unilamellar vesicles for several months. The composition and extent of these vesicles was reproducible, independent of the sample history or mixing path. These findings led to the conclusion that such a system unambiguously suggested an equilibrium system with a spontaneous curvature.[38] Other reported results, however, disagree with this proposition. Almgren and Rangelov argued that their results for a different surfactant mixture clearly showed that the spontaneous vesicle populations do not represent a system in true equilibrium and that the vesicle dispersion only represents a state of lower free-energy than the starting solutions.[42] In contrast, vesicles formed from lecithin–bile salt mixtures[43] and phospholipids are kinetically trapped dispersions of lamellar phase and so are not the equilibrium state of aggregation.[44] Recently, Nieh *et al.* reported spontaneously formed unilamellar vesicles by phospholipids with a path-dependent size distribution. Their results implied that unilamellar vesicle morphology is most likely thermodynamically stable but the size distribution depends on the equilibrium-precursor morphology.[45]

Cryo-TEM has also played a critical role in the study of elongated micellar networks. Worm-like micelles have unique rheological properties that arise from the fact that they can break and reform under shear, branch, and form networks. Scattering and rheology experiments are often able to determine the microstructure of the micelles and some network parameters; however, only cryo-TEM can unambiguously identify topological defects such as branched micelles[46–48] and micellar endcaps.[49] These topological defects of the infinite cylinders require higher curvature energy to form. However, the introduction of either an endcap or a junction increases the system entropy. Branching occurs if the energy required to create a three-fold junction is less than that needed to form a hemispherical endcap.[50,51] Experimentally, branched worm-like structures form in ternary or higher systems, *e.g.* by mixing different types of surfactants together, or in microemulsions, or at high salt concentrations in a solution of a single surfactant type.[47,48,52] The possible existence of branched micelles in a binary surfactant–solvent system was predicted in concentrated solutions of dimeric surfactants by molecular dynamic simulation.[53] This postulation was not confirmed until cryo-TEM experimental results clearly showed

the existence of branched micelles of a triquaternary ammonium (trimeric) surfactant in aqueous solution.[46] Three-fold junction structures (Y-junctions) have also been found in micelles of a high molecular weight poly(ethylene oxide)-*block*-poly(butadiene) (PEO-*b*-PB) block copolymer in aqueous solution.[54] Formation of Y-junctions in block copolymer amphiphiles was attributed to long PB blocks that are more tolerant to chain-packing distortion in complex packing geometries such as within the core of a branch point. The formation of Y-junctions between ribbon elements has also been confirmed by cryo-TEM (Fig. 2B).

The study of microstructure evolution has been improved by the use of cryo-TEM because of its ability to unequivocally describe coexisting nanostructures. The study of intermediate structures formed during vesicle–micelle transitions in mixed lipid–surfactant solutions[52,55–64] is of particular interest. Cryo-TEM provides direct evidence of the structural pathway between vesicles and micelles promoted by either the addition of surfactants into lipid-vesicle solutions or selective removal of surfactants from lipid–surfactant complex micelles. Understanding the nature of this phase transition is essential to the elucidation of biological membrane solubilization and reconstitution, the development of reconstitution protocols, and the control of drug encapsulation and release.[56] Bilayer fragments and thread-like micelles were first captured as two intermediate structures between vesicles of pure lipids and mixed lipid–surfactant spherical micelles.[55,57–60] Perforated vesicles and mesh-like intermediate structures were observed for mixtures of a cationic surfactant and lecithin vesicles.[58,65] Other studies, however, on lecithin,[60] nonionic surfactant–cholesterol mixtures[56] and dimeric gemini surfactants[66] have shown the *absence* of thread-like micelles as an intermediate structure in the vesicle–spherical micelle transition.[34]

Intermediates during the micelle to vesicle transition have also been studied in solutions containing mixed surfactants,[52,67] mixed surfactants with added salt,[68] and fluorinated surfactants with added salts.[68] Talmon and coworkers reported sequential formation of various intermediates by mixing a thread-like micelle-forming dimeric surfactant with a vesicle-forming dimeric surfactant in aqueous solution.[52] With the progressive addition of the former surfactants, vesicles first increased in size before breaking apart into smaller vesicles. Further addition resulted in the stepwise transformation into disk-like, ring-like, shorter thread-like, longer thread-like micelles, and finally an entangled thread-like micellar network.

In addition to observing transitions from micelles to vesicles, Wang *et al.* also reported the existence of bilayer sheets in equilibrium with open and closed vesicles and disk-like structures.[69] Fully developed lamellar phases have been studied by cryo-TEM and allow for visual determination of bilayer thickness and spacing.[70,71] In addition, Ponsinet and Talmon successfully imaged an L_3 sponge phase and were able to differentiate between electrostatically and sterically stabilized lamellar phases. Electrostatically stabilized lamellar sheets appeared rigid and well-ordered, while sterically stabilized lamellar sheets were characterized as soft and fluctuating.[71]

Vesicles have important applications as delivery vehicles for the formation of and/or transporting of encapsulated materials, such as drugs, nanocrystals and DNA. Encapsulated materials result in greater phase and/or mass-thickness contrast and are readily visualized by cryo-TEM.[72–75] For example, maghemite nanocrystals were synthesized and successfully encapsulated within large unilamellar vesicles formed by film hydration coupled with sequential extrusion.[72]

Cryo-TEM has also been extensively used to help interpret the 3-dimensional (3-D) structure of biomacromolecules and their complex structures because of its ability to provide high-resolution, *in situ* structure information.[8] In 3-D analysis, an object of interest is imaged at varying angles by tilting the sample, and the 3-D structure can be mathematically reconstructed from these 2-D projections. For example, nanometre-scale resolution of DNA toroids in vitreous ice provided detailed packing information of DNA organization within toroidal condensates,[76] and showed that both hexagonal and nonhexagonal DNA packing could be present within the same toroid. Cryo-TEM also finds extensive application in the imaging of lipid complex-DNA structures with the purpose of understanding the mechanism of gene therapy.[77] A complete review of this field is available.[6,78]

Macromolecular amphiphiles

Recently, amphiphilic block copolymers have been recognized as technically important solution assemblies because of properties such as a low critical micelle concentration (cmc), mechanically robust assemblies, highly tunable composition and chain architecture, selective solvent micellization, and abilities to trap unstable or metastable structure due to slow molecular dynamics.[79,80] The combination of these different features offers flexibility for developing novel assembled morphologies with well-defined structures. The aggregation behavior of block copolymers is more complicated than that of low molecular weight surfactants. Classic polymeric assemblies, such as vesicles, spherical and worm-like micelles,[22,81–83] and non-classic polymeric assemblies, such as disks,[24] toroids,[15] multicompartment micelles,[84,85] polygonal vesicles,[86] and thread-like micelles with three-fold junctions and network structures[53] have been visualized *via* cryo-TEM.

Polymeric micelles formed in aqueous solution consist of a dense core and a diffuse corona highly swollen with solvent. Sometimes, the hydrophilic corona is well-solvated and is barely directly visible by cryo-TEM. In some cases, their dimensions can be estimated by the typical separation distance between adjacent cores.[84] Core-corona structures were directly resolved for both cylindrical and spherical micelles of poly(ethylene oxide)-based block copolymers,[82,83] with Cryo-TEM images showing micelles with a dark core surrounded by a grey halo representing the PEO corona. This observation led to the conclusion that PEO segments collapse on the hydrophobic PB surface despite their favorable interactions with water. This is consistent with earlier neutron-scattering results.[87] It is noteworthy that, very recently, cryo-TEM directly imaged responsive shell structures of core–shell colloidal particles.[88,89] Wittemann *et al.* showed both extended and collapsed spherical brushes, depending on ionic strength in solution.[88] Distortion of the spherical geometry, upon the approach of two charged particles, was also shown. Crassous *et al.* demonstrated a thermo-responsive shell structure, clearly

Table 2 A brief summary of organic solvents successfully vitrified in samples imaged with cryo-TEM

Amphiphiles	Solvent	Coolant	Ref.
PAA-*b*-PMA-*b*-PS	THF–Water	Ethane	15
PS–PI cyclic	Heptane, decane	Nitrogen	16,17
PS-*b*-PI	Dioctylphthalate, dibutylphthalate, diethylphthalate and dimethylphthalate	Nitrogen	18
PS-*b*-PVP	Toluene	Nitrogen	19,20
PFDMS-*b*-PMMA	Acetone–THF	Nitrogen	21
PB-*b*-PEO	1-Butyl-3-methylimidazolium hexafluorophosphate([BMIM][PF_6]	Nitrogen	22
1,2-Polybutadiene-*b*-poly(hexafluoropropyleneoxide)	Bis(2-ethylhexyl)phthalate	Nitrogen	24
Lecithin	Soybean oil–hexane mixtures	Nitrogen	14
Lecithin–water	Isooctane	Nitrogen	25
Monoglycerides	Olive oil	Nitrogen	25
Peptides	Dimethyl formamide (DMF)	Nitrogen	26
Cationic surfactants	Water–ethylene glycol mixtures	Ethane	27
$(EO)_{15}$–$(PDMS)_{15}$–$(EO)_{15}$	Water–glycerol mixtures	Ethane	28
Heterocomplementary monomers	Isooctane	Nitrogen	29

visible in cryo-TEM images, of polystyrene–poly(*N*-isopropylacrylamine) (PS–PNIPAM) at different temperatures.[89]

The molecular level structure of block copolymers is an important design parameter for the control of the final assembled morphology. Dominant interactions during micellization are defined by choices of the hydrophilic blocks (ionic or nonionic) and hydrophobic blocks (to form a glassy or liquid core). The micelle structure of block copolymers with a hydrophobic fluid core, such as poly(butadiene) and poly(isoprene), can be probed with cryo-TEM. This gives not only the shape of polymeric aggregates but also allows size measurement (with the limitation of magnification accuracy), which subsequently provides a direct determination of the degree of chain stretching in the hydrophobic cores.[83,84]

Cryo-TEM has also been used as a major technique in the study of chain-exchange kinetics in polymeric micelle solutions. Jain and Bates reported real-space cryo-TEM images that provide direct evidence of the consequence of nonergodicity in PEO-*b*-PB micelle solutions.[90] According to their experiments, the final micelle structures depend on the mixing procedure. After initial micelle formation in solution, the micelle structures are kinetically trapped and the system is composed of locally isolated aggregates. The extremely slow kinetics of chain exchange between polymeric micelles inhibits the solution from reaching a global equilibrium, although individual micelles can still have a locally equilibrated structure with preferred dimensions. Studies of the same type of copolymers in ionic solvent *via* cryo-TEM lead to the same conclusion.[22] More recently, Danino and coworkers showed that the exchange kinetics and the stability of polymeric vesicles strongly depend on the solution composition. Using on-the-grid-processing they demonstrated that PEO-*b*-PB vesicles undergo fast dissolution, and within seconds transform into cylindrical and spherical micelles when surfactant is added. Furthermore, the newly formed mixed surfactant–polymer assemblies are equilibrium structures.[91]

Amphiphilic copolymers are not always directly soluble in pure water due to the low solubility of their hydrophobic blocks. In order to study the thermodynamic formation mechanism of these less soluble polymers, they must first be dissolved in an organic solvent and water added gradually. Using mixed solvents with different selectivity to different blocks provides a convenient way to tune polymeric micelle structure. In the case of hydrophobic core polymers with high glass transition temperatures, the assembled structures can be kinetically trapped either by dialyzing the solution against pure water or by quickly introducing a large amount of water into the solution.

Examining the *in situ* micelle structure in organic or mixed solvents leads to new problems in cryo-TEM because most organic solvents are highly soluble in liquid ethane.[14] To circumvent this complication, macromolecular samples in organic solvents are typically vitrified in liquid nitrogen. Although the cooling rates in liquid nitrogen are lower than in liquid ethane at its freezing point, liquid nitrogen can be used because many organic solvents do not crystallize readily. Table 2 briefly summarizes examples from the literature of assembled structures successfully vitrified in organic solvents. Hillmyer, Lodge, Talmon and coworkers have shown the effect of different mixtures of phthalates on the morphology of poly(styrene-*b*-isoprene) diblock copolymer aggregates, and the aggregates change from spherical micelles to thread-like micelles to vesicles. Curiously, in these systems the vitrified solvent is more electron dense than the aggregates, so the contrast in these systems is reversed compared to that of aqueous systems.[18,81] Very recently, Lodge's group demonstrated that PB-*b*-PEO diblock copolymers can also form well-defined micelles in an ionic liquid, 1-butyl-3-methylimidazolium hexafluorophosphate ([BMIM][PF_6]).[22] Thread-like micelles and an ordered lamellar phase were also shown to coexist for lecithin in isooctane (Fig. 3).[25]

Recently, a dominant toroidal micelle morphology has been produced by the self assembly of poly(acrylic acid)-*block*-poly(methyl acrylate)-*block*-polystyrene (PAA-*b*-PMA-*b*-PS) triblock copolymer *via* interaction with organic counterions in mixed THF–water solutions.[15] Ring-like micelles have been shown by cryo-TEM as a transition structure that forms initially after mixing two dimeric surfactants.[49,52] Formation of toroids *via* molecular assembly is not unprecedented in nature. Multivalent counterions can also produce toroidal bundles of DNA molecules in dilute solution.[92] Understanding the formation mechanism of toroids is critical to the understanding of *in vivo* processes, *e.g.* DNA compaction and storage in the chromosome.[93,94] Intermediate structures captured by both TEM (cast film) and cryo-TEM revealed a possible pathway by which toroids could be constructed from

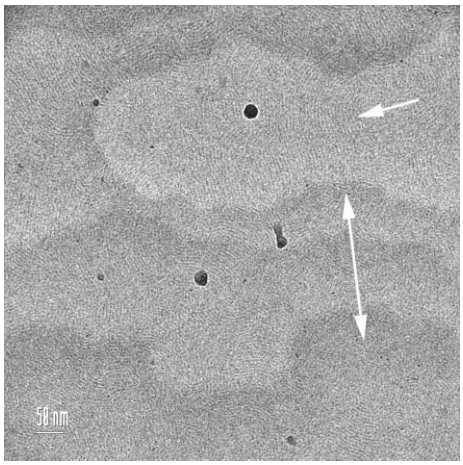

Fig. 3 Direct-imaging cryo-TEM image of 19% lecithin and 1% water (wt.) in isooctane. Note the coexistence of thread-like micelles (arrow) and a lamellar phase indicated by the step-wise change of contrast along the double-headed arrow (Y. Talmon, unpublished results).

either inter- or intra-fusion of cylindrical micelles[15]. Fig. 4A and 4B show typical cryo-TEM images of toroids in a THF–water mixture containing 40% THF by volume. The sample was vitrified in liquid ethane because water can be successfully vitrified and THF has low solubility in liquid ethane. Aging toroidal micelle solutions at room temperature for a few months, or annealing them at elevated temperature for only a few hours, results in the fusion of toroids, suggesting toroidal micelles might be long-lived, but unstable or, at most, metastable structures. Intermediate structures during this morphological evolution can be captured *via* cryo-TEM as shown in Fig. 4C and 4D.

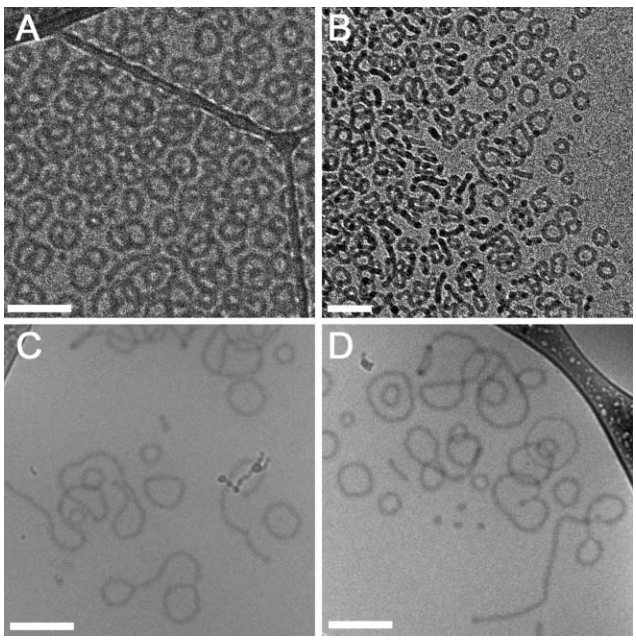

Fig. 4 Cryo-TEM image of PAA-*b*-PMA-*b*-PS triblock copolymer in mixed THF–water solvents containing 40 volume percent THF. (A) The vitrified solvent film is thin, and all the toroidal micelles are confined into the thin layer of the vitrified film. (B) The vitrified solvent film is relatively thick, allowing tilt of toroidal micelles. (C) and (D) Cryo-TEM images of intermediate structures formed during the fusion of toroids. All scale bars represent 200 nm.

The assembly behavior of hydrogels created through the self assembly of amphiphilic copolypeptides,[95] small peptides,[96] and small, hybrid peptide amphiphiles,[97,98] has also been studied with cryo-TEM. One great advantage of the hydrogels formed by amphiphilic copolypeptides or small peptides is that their rheological and morphological properties can be conveniently engineered through the adjustment of the secondary structure of the polypeptides, or by utilizing peptide intramolecular folding events.[96,99–101] The imaging of hydrogels can be challenging because they are highly swollen with water, do not yield significant mass-thickness and phase contrast, and are difficult to confine in a thin film. Fig. 5 shows a cryo-TEM image clearly demonstrating the hydrogel morphology assembled by a 20-residue peptide with the sequence of $VKVKVKVKV^{D}PPTKVKVKVKV–NH_2$.[96,100,101] In the presence of external stimuli, such as changes in pH,[96] temperature,[100] and salts,[101] the peptide is designed to undergo an intramolecular folding event to form a β-hairpin structure that consequently self assembles into long fibrils. Branching and entanglement endow the system with elastic gel properties tunable with the magnitude of folding stimulus present in solution. The cross-section of the fibrils directly observed by cryo-TEM is consistent with that measured by small-angle neutron scattering,[101] and both are equal to the size of a folded peptide sequence consistent with the proposed model of self-assembly.[96,101] Cryo-TEM imaging also allows the kinetic study of the self-assembly process by allowing the observation of fibril growth through vitrification of peptide solutions during the self-assembly process.

Freeze-fracture-replication cryo-TEM (FFR) is an excellent technique to complement direct-imaging cryo-TEM. It can be applied to image highly viscous liquids and to study liquid systems that contain large objects with nanometric details. This technique has been unjustifiably neglected by

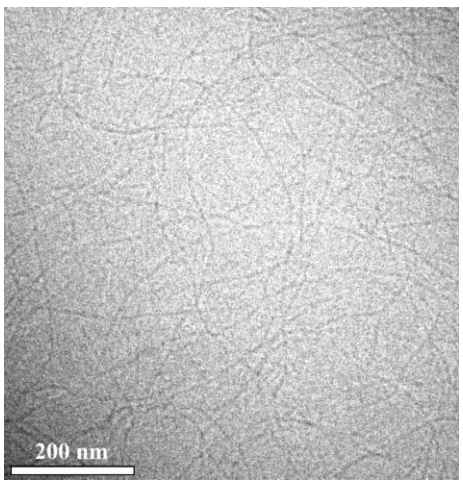

Fig. 5 Cryo-TEM image of 0.25 wt% MAX1 ($VKVKVKVKV^{D}PPTKVKVKVKV–NH_2$) gel in pH 7 buffer after 45 minutes of self assembly at 22 °C. The image clearly shows an entangled fibrillar nanostructure with a diameter equal to that of a folded peptide sequence.

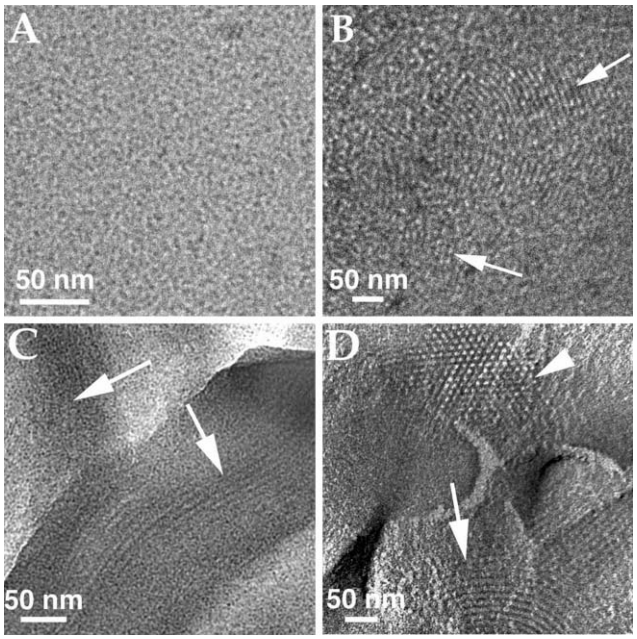

Fig. 6 A time sequence of the evolution of nanostructure resulting from the formation of SBA-15 in an acidic (HCl) solution of Pluronic P123, vitrified from 35 °C: (A) After 5 minutes 13 seconds (5:13) only spheroidal micelles are seen. (B) After 14:05, arrows show the thread-like micelles (TLMs). (C) Freeze-fracture-replication of the same system at t = 16:27, arrows point to TLMs. (D) Same at t = 21:42. The hexagonal arrangement of the TLMs in this liquid-crystalline phase is seen along their long axes (arrowhead). A different domain allows a view perpendicular to the long axis (arrow). Reprinted with permission from reference 30, Copyright 2006 American Chemical Society.

microscopists who study complex liquids; it certainly deserves a revival. Fig. 6 demonstrates the complementarity of direct-imaging cryo-TEM and freeze-fracture-replication cryo-TEM. It shows the evolution of nano structures of the mesoporous material SBA-15 from a low-viscosity micellar solution into a very viscous liquid-crystalline inverse-hexagonal phase. The reaction mixture was sampled several times after the addition of tetramethoxyorthosilane (TMOS) to an acidic (HCl) solution of Pluronic P123 held at 35 °C.[30] Fig. 6A is a direct-imaging cryo-TEM micrograph of spheroidal micelles in the system sampled after five minutes and 13 seconds (5:13). It is difficult to make out the individual micelles because of their relatively high concentration, leading to the projection of several layers of micelles in the image. Thread-like micelles (TLMs) are observed by direct-imaging cryo-TEM after 14:05 (arrows in Fig. 6B). Some of these micelles were aligned by the flow during specimen preparation, while in other areas one sees the projection of randomly oriented TLMs. This is frequently observed in cryo-micrographs of TLMs, especially at relatively high concentration. TLMs (arrows) are also seen by freeze-fracture-replication of the system at about the same time of 16:27 (Fig. 6C). The last two images indicate that the two techniques visualize the same nanostructures. As the reaction progresses, the system becomes increasingly viscous, as the liquid-crystalline phase is formed, and eventually it is impracticable to prepare direct-imaging cryo-TEM specimens; only FFR can be used. At 21:42, Fig. 6D, FFR reveals the formation of a hexagonal liquid-crystalline phase. The hexagonal arrangement of the micelles is seen along their long axes (arrowhead), while the view perpendicular to the long axis (arrow) produces in projection parallel lines.

Artifacts typically observed in cryo-TEM

Artifacts observed in cryo-TEM caused by sample preparation arise from several major sources: strong shear forces caused by blotting, solvent evaporation after blotting, the confinement of assembled structure to an ultrathin film, and solvent freezing (crystallization).[61,102–105] During blotting, samples are subjected to shear rates that can exceed 10^4 s^{-1}. Alignment of thread-like micelles and shear-induced phase transition have been reported and attributed to the strong shear force induced during the blotting process.[61,102,103] Danino *et al.* reported a shear-induced transition from thread-like micelles to bilayer-like fragments in $CPClO_3$–$NaClO_3$ mixtures caused by blotting.[61] Zheng *et al.* also observed flow-induced nanostructure transitions, *e.g.* from vesicles to thread-like micelles, due to blotting-induced shear.[104] Although high sheer rates due to blotting are unavoidable during cryo-TEM sample preparation, the effects can be mitigated by allowing adequate relaxation time after blotting. Typical relaxation times range from a few seconds to minutes. This on-the-grid relaxation may be problematic if the atmosphere in the preparation chamber is not properly saturated.

Evaporation of solvent from the thin film formed by blotting causes concentration changes and cooling. This may lead to phase transitions or the formation of artifacts not present in the original dispersion. Talmon determined that the preparation of samples in the open air always results in unacceptable levels of solvent evaporation.[105] To avoid the problem, samples must be prepared in closed devices allowing preparation under controlled temperature and humidity conditions, such as the CEVS or "Vitrobot" mentioned above. Although the Vitrobot has simplified somewhat sample preparation for certain systems, some microscopists still prefer the better flexibility afforded by the non-computerized systems. In the Vitrobot, temperature, humidity, and blotting parameters are controlled by software and blotting is carried out by automated, pneumatic pads. While the effect of evaporation is most often undesirable, carefully controlled evaporation has been used successfully as a method of "on-the-grid processing" allowing, for example, the formation of more concentrated samples and/or ordered phases.[106]

Other artifacts observed in cryo-TEM are the result of the formation of thin films. Aggregation may occur if the film thickness is comparable to the size of particles of interest in the suspension, or the concentration is high. Egelhaaf *et al.* reported a discrepancy between vesicle-size distributions obtained from cryo-TEM, freeze-fracture electron microscopy and dynamic light scattering and attributed it to aggregation of vesicles in the thin film,[107] although De Smet *et al.* found agreement between size distributions determined from light scattering and cryo-TEM.[108] As expected, the former technique gave a larger average size than the latter. Artifactual aggregation of particles may also occur in the film if the particles have a strong affinity for binding to the grid. In

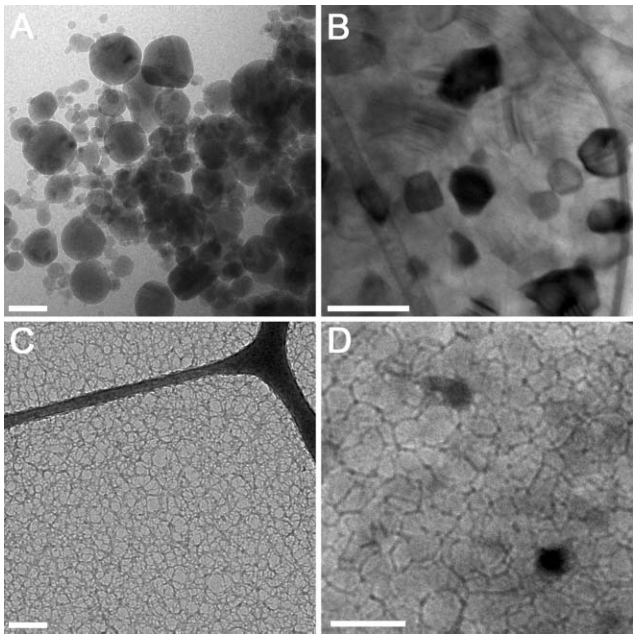

Fig. 7 Artifacts of different ice forms: (A) Large ice (frost) crystals; (B) hexagonal and truncated ice crystals. Some crystals seem extremely dark due to Bragg scattering of electrons; (C) porous dry films of vitrified water, most likely due to overblotting. Films that are too thin from overblotting are vulnerable to evaporation during the subsequent plunging and hole formation during electron-beam irradiation during imaging; (D) regular polygonal ice-crystal arrangement formed upon unsuccessful vitrification. All scale bars represent 200 nm.

addition, the thin vitrified films are not flat but rather biconcave in shape with a thin center and thicker edge (Fig. 1E and 1F). This thickness gradient can lead to preferential size sorting of structures with larger particles tending to gather at the edges of the holes, and smaller particles at the center (Fig. 1F).[109] This may also lead to concentration gradients on the grid.[1] This artifact has also been exploited as a form of "on-the-grid preparation".[106] In cases of extreme particle size, the limited thickness of the film may exclude or deform the particles. Large particles may also protrude from the film.

Successful vitrification of water is critical for aqueous cryo-TEM imaging. However, hexagonal or cubic ice crystals are occasionally encountered. Crystallization of water molecules is not desired because it could cause optical artifacts, or damage and redistribution of the assembled structures.[4] Fig. 7 shows a list of artifacts resulting from deposition of ice particles on the film, crystallization of water molecules, and drying of the film. Crystallization may arise from a relatively low cooling rate of the sample, or occur during sample transfer. At the low pressure inside the TEM, vitreous ice is not a thermodynamically stable structure but a kinetically trapped supercooled liquid. Long exposure to a high dose of electrons or heating in the TEM chamber can lead to formation of more stable forms of ice, such as cubic or hexagonal crystals. Talmon *et al.* found that electron-beam radiation damage is less severe in vitreous ice than in crystalline ice.[4,32] This damage is more severe at the interfaces between organic materials with crystalline ice.

Electron interaction with the specimen during imaging inevitably leads to the decomposition of the structures of interest (radiolysis). Electron-beam radiation is particularly severe in vitrified specimens containing significant amounts of organic compounds. The development of digital microscopy using a charge-coupled device (CCD) camera has made low-dose imaging much easier.[110] Since the electron dose for the exposure is relatively fixed, the strategy of low-dose imaging is to minimize the electron dose prior to exposure. This can be accomplished with the application of low-dose software and low-dose CCD image capture. Image shifting is also helpful in this method in order to minimize electron dose. Imaging shifting involves focusing and making astigmatism corrections first in areas adjacent to a desired sample area reached *via* an off-axis beam shift. Images are then recorded on the previously unexposed area by translating the electron beam back to the area of interest. In some cases, selective etching can be used to bring out structural details[111] or to determine whether some features are merely surface contamination, such as frost.[61]

Future prospects

The invention of controlled devices for specimen preparation and the development of CCD cameras with low-dose imaging capabilities have advanced cryo-TEM as one of the most powerful characterization tools in the field of amphiphilic self-assembly. Reports of the application of cryo-TEM to soft nanoscale materials have continued to increase in the past 16 years (Fig. 8). Recent discovery of novel structures by self assembly of block copolymers in solution all involved the usage of cryo-TEM as a major characterization method.[15,54,84]

Although cryo-TEM can provide detailed structural information on many length scales, it is not a self-sufficient technique for the study of self-assembled amphiphilic molecules. There is no doubt that the complete characterization of self-assembled amphiphiles requires complementary information gathered by traditional techniques such as small-angle X-ray and neutron scattering, light scattering, rheology measurements and nuclear magnetic resonance.

New perspectives are emerging from the study of amphiphiles in aqueous and, the emerging area of, organic solvents. When combined with the study of the application of external

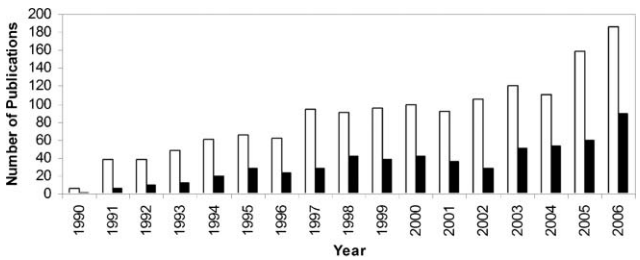

Fig. 8 Histogram of publications from 1990 to 2006 showing increased application of cryo-TEM. Data were obtained as of 2006 using the ISI 'Web of Science' database (http://portal.isiknowledge.com). In white: publications related to application of cryo-TEM (TS = (cryo* TEM or cryo*TEM or cryo* Transmission electron microscopy)); In black: publications related to the application of cryo-TEM technique in the field of amphiphiles (TS = ((cryo* TEM or cryo*TEM or cryo* Transmission electron microscopy) and (amphiphil* or surfactant* or block copolymer* or micell* or vesicle* or liposome*))). Cryo-TEM has also been used extensively in the field of biology.

stimuli and the study of kinetics, one can potentially understand the formation mechanisms of complicated solution structure in binary, ternary or higher systems. Cryo-TEM will play an important role in providing detailed structural information of complex nano-aggregates, illustrating their construction mechanisms, and consequently helping in the design of new functional materials. This will be facilitated by combining direct-imaging cryo-TEM with FFR-TEM, and by using time-resolved cryo-TEM and more on-the-grid processing for sample preparation.

Acknowledgements

DJP and HC thank the collaborating polymer and peptide synthesis labs of Karen Wooley and Joel Schneider, respectively, and Tuna Yucel for providing Fig. 5. The microscopy work of DD and YT has been done at the George and Hannah Krumholz Advanced Microscopy Laboratory, part of the Technion Project on Complex Fluids, Microstructure and Macromolecules. DJP, HC, TKH, and EMK acknowledge the W. M. Keck College of Engineering Electron Microscopy Laboratory at the University of Delaware and the assistance of Chaoying Ni, and Frank Kriss. Support for this work comes from the National Science Foundation grant DMR-0210247 and CBET-0436195, NIH R01 DE016386-01, the RBNI at Technion, and the Binational Science Foundation.

References

1 J. R. Bellare, H. T. Davis, L. E. Scriven and Y. Talmon, *J. Electron Microsc. Tech.*, 1988, **10**, 87–111.
2 P. K. Vinson, J. R. Bellare, H. T. Davis, W. G. Miller and L. E. Scriven, *J. Colloid Interface Sci.*, 1991, **142**, 74–91.
3 M. Almgren, K. Edwards and J. Gustafsson, *Curr. Opin. Colloid Interface Sci.*, 1996, **1**, 270–278.
4 Y. Talmon, in *Modern Characterization Methods of Surfactant Systems*, ed. B. P. Binks, Marcel Dekker Inc., New York, 1999, pp. 147–178.
5 D. Danino and Y. Talmon, in *Physical Chemistry of Biological Interfaces*, ed. A. Baszkin and W. Norde, Marcel Dekker Inc., New York, 2000, pp. 799–822.
6 M. Almgren, K. Edwards and G. Karlsson, *Colloids Surf., A*, 2000, **174**, 3–21.
7 Y. I. Gonzalez and E. W. Kaler, *Curr. Opin. Colloid Interface Sci.*, 2005, **10**, 256–260.
8 P. M. Frederik and N. Sommerdijk, *Curr. Opin. Colloid Interface Sci.*, 2005, **10**, 245–249.
9 Y. Y. Won, *Korean J. Chem. Eng.*, 2004, **21**, 296–302.
10 M. Antonietti and S. Forster, *Adv. Mater.*, 2003, **15**, 1323–1333.
11 J. H. Collier and P. B. Messersmith, *Annu. Rev. Mater. Res.*, 2001, **31**, 237–263.
12 V. P. Torchilin, *Nat. Rev. Drug Discovery*, 2005, **4**, 145–160.
13 D. Danino, K. H. Moon and J. E. Hinshaw, *J. Struct. Biol.*, 2004, **147**, 259–267.
14 D. Danino, R. Gupta, J. Satyavolu and Y. Talmon, *J. Colloid Interface Sci.*, 2002, **249**, 180–186.
15 D. J. Pochan, Z. Y. Chen, H. G. Cui, K. Hales, K. Qi and K. L. Wooley, *Science*, 2004, **306**, 94–97.
16 J. L. Putaux, E. Minatti, C. Lefebvre, R. Borsali, M. Schappacher and A. Deffieux, *Faraday Discuss.*, 2005, **128**, 163–178.
17 R. Borsali, E. Minatti, J. L. Putaux, M. Schappacher, A. Deffieux, P. Viville, R. Lazzaroni and T. Narayanan, *Langmuir*, 2003, **19**, 6–9.
18 E. Kesselman, Y. Talmon, J. Bang, S. Abbas, Z. B. Li and T. P. Lodge, *Macromolecules*, 2005, **38**, 6779–6781.
19 G. T. Oostergetel, F. J. Esselink and G. Hadziioannou, *Langmuir*, 1995, **11**, 3721–3724.
20 F. J. Esselink, E. Dormidontova and G. Hadziioannou, *Macromolecules*, 1998, **31**, 2925–2932.
21 I. Korczagin, M. A. Hempenius, R. G. Fokkink, M. A. C. Stuart, M. Al-Hussein, P. H. H. Bomans, P. M. Frederik and G. J. Vancso, *Macromolecules*, 2006, **39**, 2306–2315.
22 Y. Y. He, Z. B. Li, P. Simone and T. P. Lodge, *J. Am. Chem. Soc.*, 2006, **128**, 2745–2750.
23 D. Danino, Y. Talmon, L. E. Carpenter and W. Chen, *Abst. Pap. Am. Chem. Soc.*, 1998, **215**, U411–U411.
24 W. F. Edmonds, Z. B. Li, M. A. Hillmyer and T. P. Lodge, *Macromolecules*, 2006, **39**, 4526–4530.
25 Y. Talmon, unpublished data.
26 J. Slager, Y. Cohen, R. Khalfin, Y. Talmon and A. J. Domb, *Macromolecules*, 2003, **36**, 2999–3000.
27 Y. Zhang, J. Schmidt, Y. Talmon and J. L. Zakin, *J. Colloid Interface Sci.*, 2005, **286**, 696–709.
28 Y. Yan, H. Hoffmann, M. Drechsler, Y. Talmon and E. Makarsky, *J. Phys. Chem. B*, 2006, **110**, 5621–5626.
29 E. Buhler, S. J. Candau, J. Schmidt, Y. Talmon, E. Kolomiets and J. M. Lehn, *J. Polym. Sci., Part B: Polym. Phys.*, 2007, **45**, 103–115.
30 S. Ruthstein, J. Schmidt, E. Kesselman, Y. Talmon and D. Goldfarb, *J. Am. Chem. Soc.*, 2006, **128**, 3366–3374.
31 http://www.vitrobot.com.
32 A. H. Falls, S. T. Wellinghoff, Y. Talmon and E. L. Thomas, *J. Mater. Sci.*, 1983, **18**, 2752–2764.
33 D. P. Siegel, W. J. Green and Y. Talmon, *Biophys. J.*, 1994, **66**, 402–414.
34 D. Danino, A. Kaplun, D. Lichtenberg, Y. Talmon and R. Zana, *Abst. Pap. Am. Chem. Soc.*, 1998, **216**, U677–U677.
35 *CRC Handbook of Chemistry and Physics*, ed. D. R. Lide, CRC press, Inc., Boca Raton, 71st edn, 1990.
36 D. J. Iampietro, L. L. Brasher, E. W. Kaler, A. Stradner and O. Glatter, *J. Phys. Chem. B*, 1998, **102**, 3105–3113.
37 D. Danino, unpublished data.
38 H. T. Jung, S. Y. Lee, E. W. Kaler, B. Coldren and J. A. Zasadzinski, *Proc. Natl. Acad. Sci. U. S. A.*, 2002, **99**, 15318–15322.
39 B. Coldren, R. van Zanten, M. J. Mackel, J. A. Zasadzinski and H. T. Jung, *Langmuir*, 2003, **19**, 5632–5639.
40 H. T. Jung, B. Coldren, J. A. Zasadzinski, D. J. Iampietro and E. W. Kaler, *Proc. Natl. Acad. Sci. U. S. A.*, 2001, **98**, 1353–1357.
41 K. Horbaschek, H. Hoffmann and J. C. Hao, *J. Phys. Chem. B*, 2000, **104**, 2781–2784.
42 M. Almgren and S. Rangelov, *Langmuir*, 2004, **20**, 6611–6618.
43 J. Leng, S. U. Egelhaaf and M. E. Cates, *Biophys. J.*, 2003, **85**, 1624–1646.
44 E. F. Marques, *Langmuir*, 2000, **16**, 4798–4807.
45 M. P. Nieh, V. A. Raghunathan, S. R. Kline, T. A. Harroun, C. Y. Huang, J. Pencer and J. Katsaras, *Langmuir*, 2005, **21**, 6656–6661.
46 D. Danino, Y. Talmon, H. Levy, G. Beinert and R. Zana, *Science*, 1995, **269**, 1420–1421.
47 Z. Lin, *Langmuir*, 1996, **12**, 1729–1737.
48 A. Bernheim-Groswasser, T. Tlusty, S. A. Safran and Y. Talmon, *Langmuir*, 1999, **15**, 5448–5453.
49 A. Bernheim-Groswasser, R. Zana and Y. Talmon, *J. Phys. Chem. B*, 2000, **104**, 4005–4009.
50 T. Tlusty and S. A. Safran, *J. Phys.: Condens. Matter*, 2000, **12**, A253–A262.
51 T. Tlusty and S. A. Safran, *Science*, 2000, **290**, 1328–1331.
52 A. Bernheim-Groswasser, R. Zana and Y. Talmon, *J. Phys. Chem. B*, 2000, **104**, 12192–12201.
53 S. Karaborni, K. Esselink, P. A. J. Hilbers, B. Smit, J. Karthauser, N. M. Vanos and R. Zana, *Science*, 1994, **266**, 254–256.
54 S. Jain and F. S. Bates, *Science*, 2003, **300**, 460–464.
55 A. Walter, P. K. Vinson, A. Kaplun and Y. Talmon, *Biophys. J.*, 1991, **60**, 1315–1325.
56 M. Seras, K. Edwards, M. Almgren, G. Carlson, M. Ollivon and S. Lesieur, *Langmuir*, 1996, **12**, 330–336.
57 P. K. Vinson, Y. Talmon and A. Walter, *Biophys. J.*, 1989, **56**, 669–681.
58 K. Edwards, J. Gustafsson, M. Almgren and G. Karlsson, *J. Colloid Interface Sci.*, 1993, **161**, 299–309.

59 K. Edwards, M. Almgren, J. Bellare and W. Brown, *Langmuir*, 1989, **5**, 473–478.
60 M. Silvander, G. Karlsson and K. Edwards, *J. Colloid Interface Sci.*, 1996, **179**, 104–113.
61 D. Danino, Y. Talmon and R. Zana, *Colloids Surf., A*, 2000, **169**, 67–73.
62 S. Rossi, G. Karlsson, S. Ristori, G. Martini and K. Edwards, *Langmuir*, 2001, **17**, 2340–2345.
63 T. H. Callisen and Y. Talmon, *Biochemistry*, 1998, **37**, 10987–10993.
64 O. Lambert, D. Levy, J. L. Ranck, G. Leblanc and J. L. Rigaud, *Biophys. J.*, 1998, **74**, 918–930.
65 M. Almgren, *Biochim. Biophys. Acta*, 2000, **1508**, 146–163.
66 D. Danino, Y. Talmon and R. Zana, *J. Colloid Interface Sci.*, 1997, **185**, 84–93.
67 E. F. Marques, O. Regev, A. Khan, M. D. Miguel and B. Lindman, *J. Phys. Chem. B*, 1999, **103**, 8353–8363.
68 J. Oberdisse, O. Regev and G. Porte, *J. Phys. Chem. B*, 1998, **102**, 1102–1108.
69 K. Wang, G. Karlsson, M. Almgren and T. Asakawa, *J. Phys. Chem. B*, 1999, **103**, 9237–9246.
70 A. Sein, J. F. L. Vanbreemen and J. Engberts, *Langmuir*, 1995, **11**, 3565–3571.
71 V. Ponsinet and Y. Talmon, *Langmuir*, 1997, **13**, 7287–7292.
72 M. S. Martina, J. P. Fortin, C. Menager, O. Clement, G. Barratt, C. Grabielle-Madelmont, F. Gazeau, V. Cabuil and S. Lesieur, *J. Am. Chem. Soc.*, 2005, **127**, 10676–10685.
73 D. D. Lasic, B. Ceh, M. C. A. Stuart, L. Guo, P. M. Frederik and Y. Barenholz, *Biochim. Biophys. Acta*, 1995, **1239**, 145–156.
74 P. P. Ghoroghchian, J. J. Lin, A. K. Brannan, P. R. Frail, F. S. Bates, M. J. Therien and D. A. Hammer, *Soft Matter*, 2006, **2**, 973–980.
75 E. Ramsay, J. Alnajim, M. Anantha, A. Taggar, A. Thomas, K. Edwards, G. Karlsson, M. Webb and M. Bally, *Pharm. Res.*, 2006, **23**, 2799–2808.
76 N. V. Hud and K. H. Downing, *Proc. Natl. Acad. Sci. U. S. A.*, 2001, **98**, 14925–14930.
77 S. Weisman, D. Hirsch-Lerner, Y. Barenholz and Y. Talmon, *Biophys. J.*, 2004, **87**, 609–614.
78 V. Alfredsson, *Curr. Opin. Colloid Interface Sci.*, 2005, **10**, 269–273.
79 T. P. Lodge, *Macromol. Chem. Phys.*, 2003, **204**, 265–273.
80 H. G. Cui, Z. Y. Chen, K. L. Wooley and D. J. Pochan, *Macromolecules*, 2006, **39**, 6599–6607.
81 J. Bang, S. M. Jain, Z. B. Li, T. P. Lodge, J. S. Pedersen, E. Kesselman and Y. Talmon, *Macromolecules*, 2006, **39**, 1199–1208.
82 Y. Zheng, Y. Y. Won, F. S. Bates, H. T. Davis, L. E. Scriven and Y. Talmon, *J. Phys. Chem. B*, 1999, **103**, 10331–10334.
83 Y. Y. Won, A. K. Brannan, H. T. Davis and F. S. Bates, *J. Phys. Chem. B*, 2002, **106**, 3354–3364.
84 Z. B. Li, E. Kesselman, Y. Talmon, M. A. Hillmyer and T. P. Lodge, *Science*, 2004, **306**, 98–101.
85 Z. B. Li, M. A. Hillmyer and T. P. Lodge, *Langmuir*, 2006, **22**, 9409–9417.
86 Z. B. Li, M. A. Hillmyer and T. P. Lodge, *Nano Lett.*, 2006, **6**, 1245–1249.
87 Y. Y. Won, H. T. Davis, F. S. Bates, M. Agamalian and G. D. Wignall, *J. Phys. Chem. B*, 2000, **104**, 7134–7143.
88 A. Wittemann, M. Drechsler, Y. Talmon and M. Ballauff, *J. Am. Chem. Soc.*, 2005, **127**, 9688–9689.
89 J. J. Crassous, M. Ballauff, M. Drechsler, J. Schmidt and Y. Talmon, *Langmuir*, 2006, **22**, 2403–2406.
90 S. Jain and F. S. Bates, *Macromolecules*, 2004, **37**, 1511–1523.
91 N. Dan, K. Shimoni, V. Pata and D. Danino, *Langmuir*, 2006, **22**, 9860–9865.
92 V. A. Bloomfield, *Curr. Opin. Struct. Biol.*, 1996, **6**, 334–341.
93 V. A. Bloomfield, *Biopolymers*, 1997, **44**, 269–282.
94 V. A. Bloomfield, *Biopolymers*, 1991, **31**, 1471–1481.
95 D. J. Pochan, L. Pakstis, B. Ozbas, A. P. Nowak and T. J. Deming, *Macromolecules*, 2002, **35**, 5358–5360.
96 J. P. Schneider, D. J. Pochan, B. Ozbas, K. Rajagopal, L. Pakstis and J. Kretsinger, *J. Am. Chem. Soc.*, 2002, **124**, 15030–15037.
97 S. E. Paramonov, H. W. Jun and J. D. Hartgerink, *Biomacromolecules*, 2006, **7**, 24–26.
98 S. E. Paramonov, H. W. Jun and J. D. Hartgerink, *J. Am. Chem. Soc.*, 2006, **128**, 7291–7298.
99 A. P. Nowak, V. Breedveld, L. Pakstis, B. Ozbas, D. J. Pine, D. Pochan and T. J. Deming, *Nature*, 2002, **417**, 424–428.
100 D. J. Pochan, J. P. Schneider, J. Kretsinger, B. Ozbas, K. Rajagopal and L. Haines, *J. Am. Chem. Soc.*, 2003, **125**, 11802–11803.
101 B. Ozbas, J. Kretsinger, K. Rajagopal, J. P. Schneider and D. J. Pochan, *Macromolecules*, 2004, **37**, 7331–7337.
102 T. M. Clausen, P. K. Vinson, J. R. Minter, H. T. Davis, Y. Talmon and W. G. Miller, *J. Phys. Chem. B*, 1992, **96**, 474–484.
103 S. L. Keller, P. Boltenhagen, D. J. Pine and J. A. Zasadzinski, *Phys. Rev. Lett.*, 1998, **80**, 2725–2728.
104 Y. Zheng, Z. Lin, J. L. Zakin, Y. Talmon, H. T. Davis and L. E. Scriven, *J. Phys. Chem. B*, 2000, **104**, 5263–5271.
105 Y. Talmon, *Colloids Surf.*, 1986, **19**, 237–248.
106 D. Danino, Y. Talmon and R. Zana, *J. Colloid Interface Sci.*, 1997, **186**, 170–179.
107 S. U. Egelhaaf, M. Muller and P. Schurtenberger, *Langmuir*, 1998, **14**, 4345–4349.
108 Y. De Smet, D. Danino, L. Deriemaeker, Y. Talmon and R. Finsy, *Langmuir*, 2000, **16**, 961–967.
109 I. Harwigsson, O. Soderman and O. Regev, *Langmuir*, 1994, **10**, 4731–4734.
110 D. Danino, A. Bernheim-Groswasser and Y. Talmon, *Colloids Surf., A*, 2001, **183**, 113–122.
111 K. Mortensen and Y. Talmon, *Macromolecules*, 1995, **28**, 8829–8834.